Chaos, Solitons and Fractals 151 (2021) 111228

Contents lists available at ScienceDirect

Chaos, Solitons and Fractals

Nonlinear Science, and Nonequilibrium and Complex Phenomena

journal homepage: www.elsevier.com/locate/chaos

A novel underdamped continuous unsaturation bistable stochastic resonance method and its application

Mengdi Li[a], Peiming Shi[a,*], Wenyue Zhang[a], Dongying Han[b]

[a] School of Electrical Engineering, Yanshan University, Qinhuangdao, Hebei 066004, P. R. China
[b] School of Vehicles and Energy, Yanshan University, Qinhuangdao, Hebei 066004, P. R. China

ARTICLE INFO

Article history:
Received 1 April 2021
Revised 29 June 2021
Accepted 29 June 2021
Available online 11 July 2021

Key words:
Stochastic resonance
Signal to noise ratio
Continuous unsaturation
Amplitude gain

ABSTRACT

In view of the saturation problem of classical bistable stochastic resonance (CBSR) system, an underdamped continuous unsaturation bistable stochastic resonance (UCUBSR) system is investigated and the feasibility of the system for weak fault feature extraction is discussed. Firstly, based on the reason of saturation phenomenon, a new potential function is constructed, which can independently adjust the steepness of the potential walls. The signal to noise ratio (SNR) of the system is derived. Secondly, a modified unsaturation index, amplitude gain, is proposed, and the influence of the steepness on SR based on SNR and amplitude gain is analyzed. The simulation analysis shows that the amplitude gain can be considered as an appropriate index to quantify SR and has a certain compensation effect on the SNR applied to evaluate unsaturation performance. Finally, from the simulation and experiment, a larger amplitude gain indicates that the proposed system has better unsaturation and weak fault detection ability compared with unsaturation bistable stochastic resonance (UBSR), and a higher amplitude of the output signal at the characteristic frequency proves that the amplitude gain as an indicator can further guide the parameter adjustment of SR and facilitate faint fault signature identification.

1. Introduction

Stochastic resonance (SR) was first proposed by Benzi to analyze the phenomenon of global climate change during glacial period [1]. Subsequently, due to the unique advantage that SR can enhance the characteristics of weak signals by noise, SR has been widely used in many fields, such as physics [2], neurology [3], medicine [4], ecology [5], especially signal processing [6-8].

Nowadays, the most widely used model is the classical bistable stochastic resonance (CBSR) system, but there is saturation in CBSR, which limits the ability of the model to enhance the characteristics of input signals [9]. Therefore, some scholars have studied the saturation problem of CBSR model. The structure of potential function affects the output of SR [10,11]. The saturation problem can be improved by linearizing the well walls on both sides of the potential function [12,13]. Qiao [14] established a piecewise bistable potential model to overcome output saturation. Experimental results showed that compared with CBSR system, the proposed system can obtain higher SNR and enhance the feature of weak signal better. Zhang [15] proposed a novel piecewise nonlinear bistable SR model. Based on the increased SNR, it is proved that the proposed system was superior to CBSR system in fault feature extraction. Li [16] constructed an improved piecewise unsaturated bistable potential model, which can better alleviate the saturation problem and obtain a bigger output SNR. These models are based on the improved potential function of CBSR, by changing the structure of both sides of the potential well to alleviate the degree of saturation. However, they are all overdamped SR models, and it is well known that the first-order SR system is equivalent to a filter in signal processing and the output of the second-order system equation is equivalent to the secondary filtering. So, the second-order SR system has better filtering effect [17-19]. Zhang [20] studied a second-order underdamped tristable SR model can realize the weak fault feature extraction much better compared with traditional tristable SR model. Li [21] proposed a multi-parameter constrained potential underdamped SR method and affirmed the effectiveness of the proposed method. However, there is little research on the underdamped unsaturation bistable stochastic resonance system. In view of this, it is necessary to study the above system.

An interesting thing is that it is different from the traditional weak signal detection method to obtain the de-noising signal by suppressing noise. SR is to transfer the high-frequency noise energy to useful signal to improve the SNR by utilizing noise. Noise

* Corresponding author.
E-mail address: spm@ysu.edu.cn (P. Shi).

https://doi.org/10.1016/j.chaos.2021.111228
0960-0779/

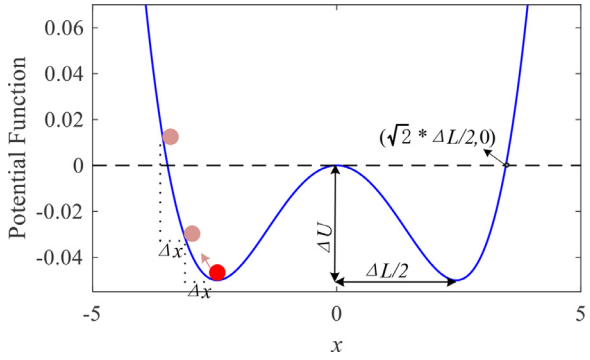

Fig. 1. Potential function in CBSR system.

is not only an important research object of weak signal processing, but also plays a vital role in other physical models [22-24].

When the system parameters, noise and input signal work together, the SR phenomenon occurs. In the actual situation, the input signal with noise has been determined, so the selection of system parameters to trigger SR is very important. There needs to be an index to quantify SR. In addition to the most commonly used SNR [25-28], there have also been other indicators for evaluating SR [29-31]. Huang [32] designed a new quantitative indicator piecewise mean value to qualify the performance of the nonlinear system response. He [33] employed the statistical complexity measure and the normalized Shannon entropy to evaluate SR of the time-delayed bistable system and verified the effectiveness of these two indexes. Xu [34] derived the spectrum amplification formula and used it to quantify the SR effect. Therefore, based on the mechanism of saturation phenomenon in CBSR system, an appropriate index can be proposed to evaluate the unsaturation ability of the system more accurately, and the system parameters need to be adjusted effectively based on the index. Due to the complexity of manual parameter adjustment, adopting intelligent optimization algorithm to search the optimal solution in rotating machine fault detection is more advantageous [35-38].

The rest of this paper is organized as follows: in Section 2, the saturation of CBSR is studied, the underdamped continuous unsaturation bistable stochastic resonance (UCUBSR) method is proposed, and the SNR of the system is derived. In Section 3, a new unsaturation evaluation index is proposed, and the relationship between this index and SR phenomenon is studied. In Section 4, the unsaturation ability of the proposed system and the significance of the proposed index are proved from both simulation and experiment. The conclusion is given in Section 5.

2. Underdamped continuous unsaturation bistable SR system

2.1. Saturation phenomenon

Langevin equation was originally used to represent the transition of Brownian particle in nonlinear system under the action of random and periodic forces, which can describe CBSR system as follows

$$\begin{cases} \frac{dx}{dt} + \frac{dU_c(x)}{dx} = S(t) + \eta(t) \\ U_c(x) = -\frac{a}{2}x^2 + \frac{b}{4}x^4 \end{cases} \tag{1}$$

where $U_c(x)$ is the potential function, a and b are the system parameters, $S(t) = A\sin(2\pi ft + \varphi)$ is the periodic signal with amplitude A, frequency f and phase φ, and $\eta(t) = \sqrt{2D}\xi(t)$ is the Gaussian white noise with $(\langle \eta(t) \rangle = 0, \langle \eta(t)\eta(t+\tau) \rangle = 2D\delta(\tau))$, where τ is time delay and D is noise intensity. The structure of the potential function is shown in Fig. 1. The barrier height and the potential spacing are $\Delta U = a^2/4b$, $\Delta L = 2\sqrt{a/b}$, and the abscissa of intersection of the right potential function and the x-axis is $\sqrt{2} * \Delta L/2$.

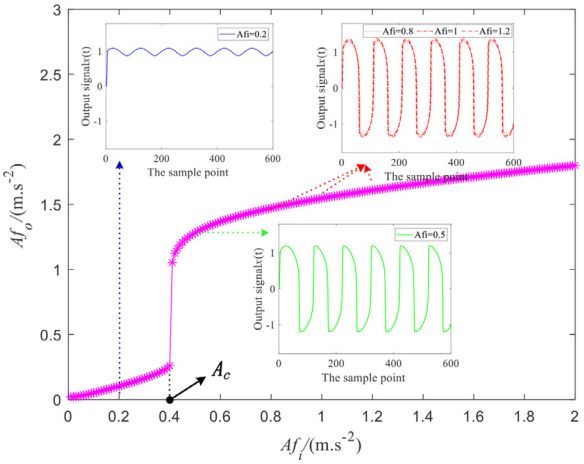

Fig. 2. Response of CBSR system with external periodic excitation only.

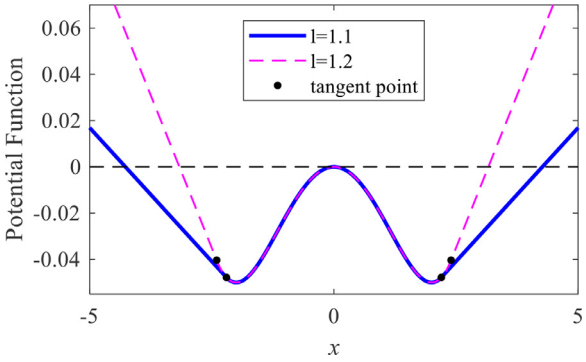

Fig. 3. Potential function in UCUBSR system.

If there exists only external periodic excitation in the system, $A_c \approx \sqrt{4a^3/(27b)}$ is a critical value for the occurrence of SR. When input signal amplitude $A < A_c$, the particle only makes local periodic oscillation motion near the potential well $x_- = -\sqrt{a/b}$ or $x_+ = \sqrt{a/b}$ on one side, and the one in the two wells is determined based on the initial value. When $A > A_c$, the particle can realize the transition between the two potential wells and make periodic motion in the two potential wells. When A continues to increase, the particle moves along the edge potential well wall. The slight motion of the particle needs to overcome the large potential energy due to the existence of potential function x^4. In terms of the potential function structure in Fig. 1, the solid sphere represents the particle. As the particle moves from the bottom of the well to the wall of the well, the higher the vertical distance is needed to move the same Δx, which limits the output amplitude of the CBSR model and results in saturation.

Fig. 2 shows the response amplitude (Af_o) of CBSR system with external periodic excitation amplitude (Af_i) only and briefly reflects the effect of potential function structure on system output. The system parameters are fixed as $a = 1, b = 1$, and $A_c \approx 0.385$ in this system. In this figure, with the increase of Af_i, the particle transits from the oscillation in the right well (when Af_i=0.2) to the transition between the left and right wells (when Af_i=0.5), and then the system response gradually falls into saturation state (when Af_i=0.8,1,1.2). After saturation, the Af_o of the system no longer increases with the increase of the Af_i. This makes the CBSR system lose weak characteristic enhancement ability.

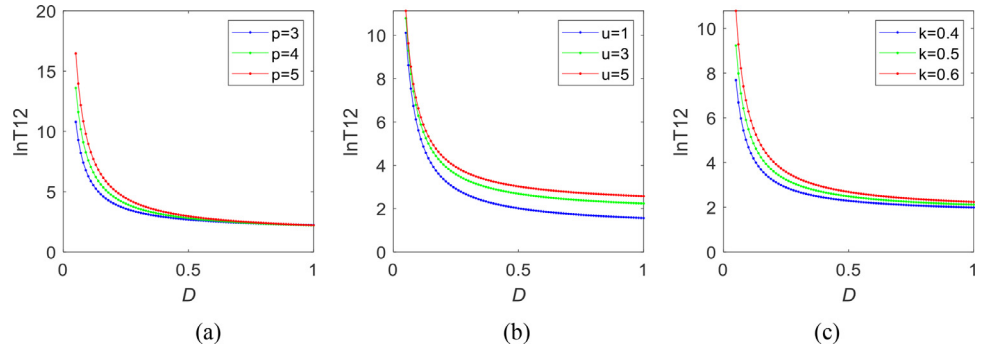

Fig. 4. MFPT versus noise intensity D for different system parameters with (a) $u = 3$ and $k = 0.6$ (b) $p = 3$ and $k = 0.6$ (c) $p = 3$ and $u = 3$.

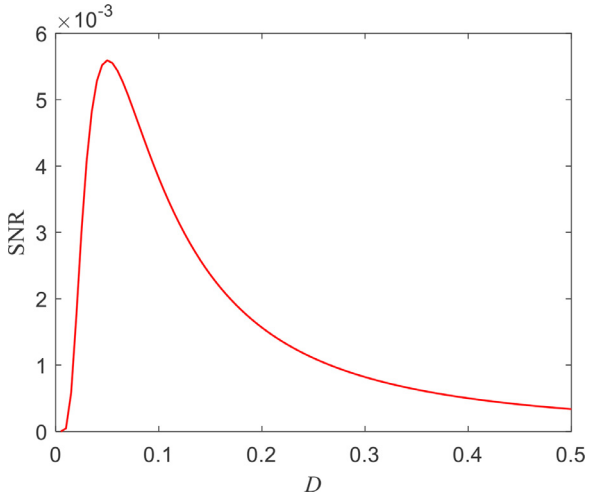

Fig. 5. SNR versus noise intensity D with $A = 0.05$, $f = 0.01$, $p = 1$, $u = 5$ and $k = 0.4$.

2.2. Potential function model and SNR derivation of UCUBSR system

To make up for the defect of CBSR saturation, an underdamped continuous unsaturation bistable stochastic resonance (UCUBSR) system is proposed, and it is controlled by the following differential equation.

$$\frac{\mathrm{d}^2x}{\mathrm{d}t} = -\frac{\mathrm{d}U(x)}{\mathrm{d}x} - k\frac{\mathrm{d}x}{\mathrm{d}t} + S(t) + \eta(t) \tag{2}$$

where k is the damping factor. The continuous potential function $U(x)$ of UCUBSR system can be written as

$$U(x) = \begin{cases} -k_d(x + x_d) + y_d & x < -x_d \\ -\frac{px^2}{2u} + \frac{px^4}{4u^2} & -x_d \le x \le x_d \\ k_d(x - x_d) + y_d & x_d < x \end{cases} \tag{3}$$

where

$$\begin{cases} x_d = l\Delta L/2 \quad 1 < l < \sqrt{2} \\ k_d = -\frac{px_d}{u} + \frac{px_d{}^3}{u^2} \\ y_d = -\frac{px_d{}^2}{2u} + \frac{px_d{}^4}{4u^2} \end{cases} \tag{4}$$

In this model, p, u, l are the system parameters, k_d is the slope of the tangent point (x_d, y_d). l is the steepness of the potential function, and the potential function structure of UCUBSR system for different l is shown in Fig. 3. The potential function model realizes the independent adjustment of barrier height $\Delta U = p/4$, potential distance $\Delta L = 2\sqrt{u}$ and steepness l.

Then, for the convenience of deriving the SNR of the system, the Eq. (2) can be simplified as

$$\begin{cases} \frac{\mathrm{d}x}{\mathrm{d}t} = y \\ \frac{\mathrm{d}y}{\mathrm{d}t} = -\frac{\mathrm{d}U}{\mathrm{d}x} - ky + A\cos(\Omega t) + \sqrt{2D}\delta(t) \end{cases} \tag{5}$$

Let $\frac{\mathrm{d}x}{\mathrm{d}t}, \frac{\mathrm{d}y}{\mathrm{d}t}, A, D = 0$, three singularities of the system of equation $(x_-, y_-) = (-\sqrt{u}, 0)$, $(x_0, y_0) = (0, 0)$, $(x_+, y_+) = (\sqrt{u}, 0)$ are acquired, and the corresponding linearization matrix is as follows [39]:

$$R_x = \begin{bmatrix} 0 & 1 \\ M_x & k \end{bmatrix} \tag{6}$$

where three singularities corresponding to M_x can be expressed as $M_{x_-} = -2p/u, M_{x_0} = p/u, M_{x_+} = -2p/u$. The singular values are linearized respectively.

$$\begin{cases} \beta_{1,2} = \left(-k \pm \sqrt{k^2 - 8p/u}\right)/2 & x = x_- \\ \lambda_{1,2} = \left(-k \pm \sqrt{k^2 + 4p/u}\right)/2 & x = x_0 \\ \beta_{3,4} = \left(-k \pm \sqrt{k^2 - 8p/u}\right)/2 & x = x_+ \end{cases} \tag{7}$$

According to Fokker-Planck equation, the probability density $\rho(x, y, t)$ of particle motion can be expressed as

$$\begin{aligned} \frac{\partial\rho(x,y,t)}{\partial t} &= -\frac{\partial}{\partial x}[y\rho(x,y,t)] \\ &\quad -\frac{\partial}{\partial y}\left[\left(-ky + A\cos(\Omega t) - \frac{\mathrm{d}U}{\mathrm{d}x}\right)\rho(x,y,t)\right] \\ &\quad +D\frac{\partial^2}{\partial y^2}\rho(x,y,t) \end{aligned} \tag{8}$$

Based on the adiabatic approximation theory [40], the distribution function of quasi steady state can be expressed as

$$\rho_{st}(x, y, t) = \bar{N}\exp\left[-\frac{\tilde{U}(x, y, t)}{D}\right] \tag{9}$$

where $\bar{N}$ is the normalized constant and $\tilde{U}(x, y, t)$ is the generalized potential well function obtained by small parameter expansion.

$$\tilde{U}(x,y,t) = \frac{k}{2}y^2 + k\int[U'(x) - xA\cos(\Omega t)]\mathrm{d}x = \frac{ky^2}{2} - kAx\cos(\Omega t) + k\begin{cases} -k_d(x + x_d) + y_d & x < -x_d \\ -\frac{px^2}{2u} + \frac{px^4}{4u^2} & -x_d \le x \le x_d \\ k_d(x - x_d) + y_d & x_d < x \end{cases} \tag{10}$$

Then, the probability transfer rate between the two potential wells can be written as follows:

$$R_\pm(t) = \frac{\sqrt{\beta_1\beta_2}}{2\pi}\sqrt{-\frac{\lambda_1}{\lambda_2}}\exp\left(\frac{-\tilde{U}(x_0, y_0, t) + \tilde{U}(x_\pm, y_\pm, t)}{D}\right) \tag{11}$$

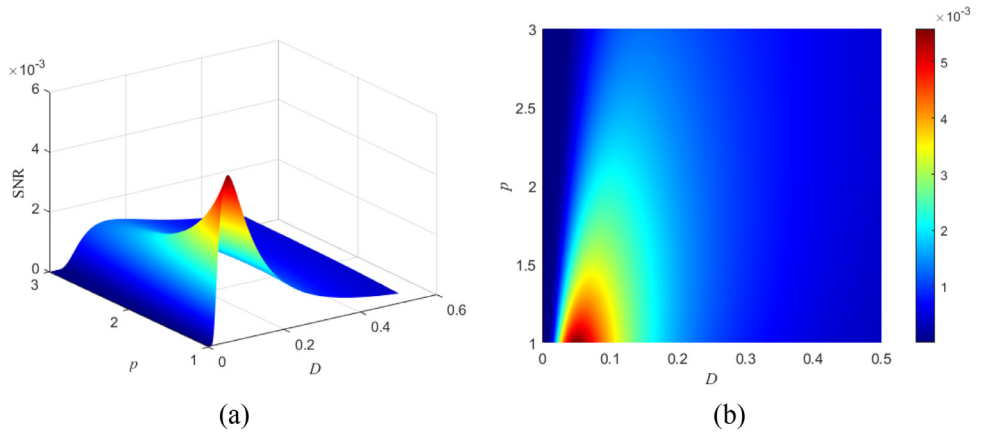

Fig. 6. SNR as a function of the noise intensity D and the system parameter p with $A = 0.05$, $f = 0.01$, $u = 5$ and $k = 0.4$.

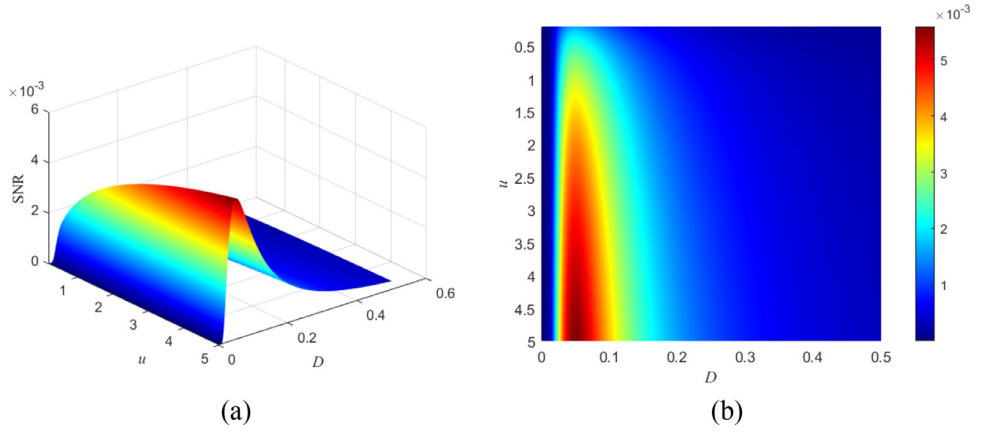

Fig. 7. SNR as a function of the noise intensity D and the system parameter u with $A = 0.05$, $f = 0.01$, $p = 1$ and $k = 0.4$.

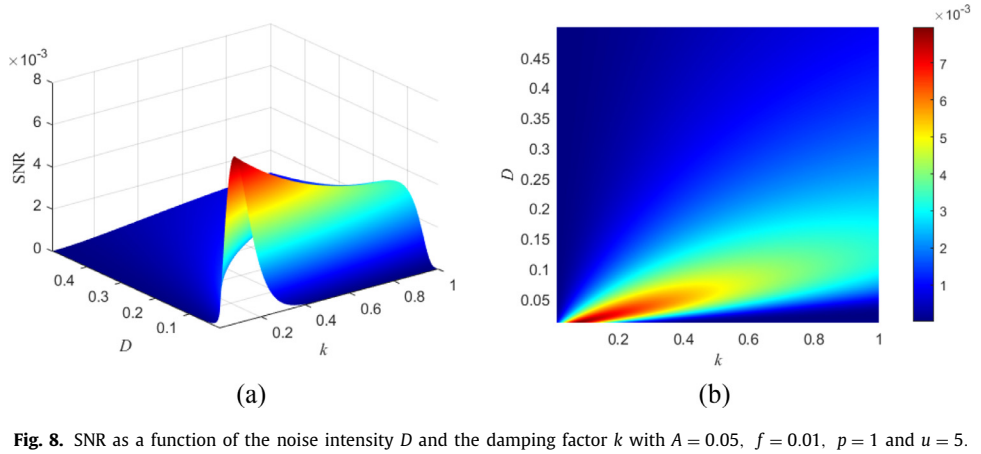

Fig. 8. SNR as a function of the noise intensity D and the damping factor k with $A = 0.05$, $f = 0.01$, $p = 1$ and $u = 5$.

The mean first passage time (MFPT) of the UCUBSR system can be obtained as

$$T12(x_+ \to x_-) = 1/R_+ \tag{12}$$

$T21(x_- \to x_+) = T12(x_+ \to x_-)$ due to the symmetric generalized potential function when the value of Ωt is $\pi/2$.

$R_\pm(t)$ after Taylor expansion, there is

$$R_\pm(t) = \frac{\sqrt{\beta_1\beta_2}}{2\pi}\sqrt{-\frac{\lambda_1}{\lambda_2}}\exp\left(-\frac{kp}{4D}\right)\Big[1 \mp \sqrt{u}A\cos(\Omega t) + \frac{1}{2}\left(\sqrt{u}A\cos(\Omega t)\right)^2 \mp \cdots\Big] \tag{13}$$

Let $R_0 = \frac{\sqrt{\beta_1\beta_2}}{2\pi}\sqrt{-\frac{\lambda_1}{\lambda_2}}\exp(-\frac{kp}{4D})$, the system output power is

$$S(\mathrm{w}) = S_1(w) + S_2(w) \tag{14}$$

where $S_1(w)$, $S_2(w)$ is the power spectrum of signal and noise respectively. Let $R_1\beta = kR_0x_+\frac{A}{D}$, $S_1(w)$, $S_2(w)$can be expressed as follows:

$$\begin{cases} S_1(\mathrm{w}) = \frac{\pi {x_\pm}^2 (R_1\beta)^2}{2\left({R_0}^2+\Omega^2\right)}[\delta(w-\Omega)+\delta(w+\Omega)] \\ S_2(\mathrm{w}) = \left[1 - \frac{(R_1\beta)^2}{2\left({R_0}^2+\Omega^2\right)}\right]\frac{2{x_\pm}^2R_0}{{R_0}^2+\Omega^2} \end{cases} \tag{15}$$

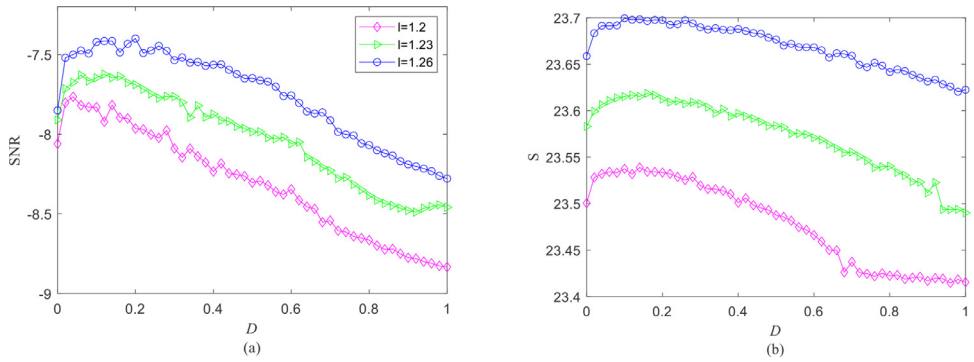

Fig. 9. The relationship between the output SNR, amplitude gain S and noise intensity D for different parameter l. $A = 0.5$, $f = 0.01$, $p = 0.1$, $u = 1$ and $k = 0.04$ (a) SNR (b) S.

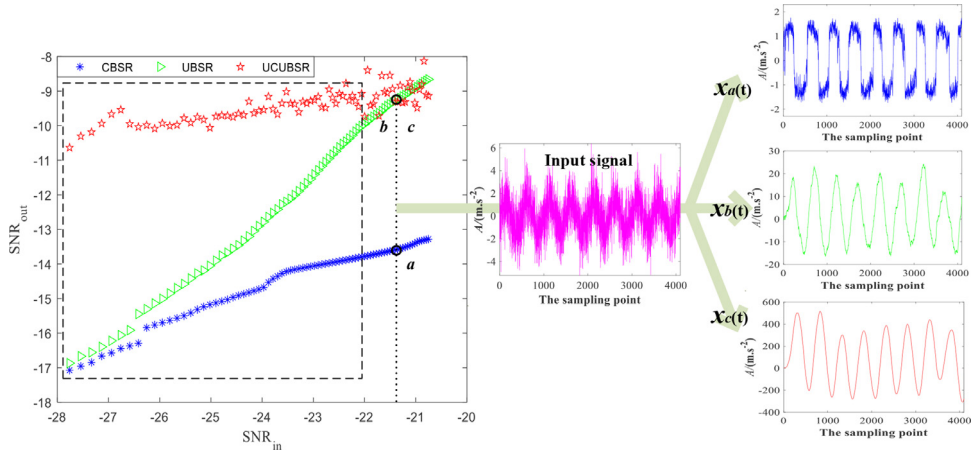

Fig. 10. The unsaturation performance analysis based on SNR.

Finally, the SNR can be expressed as:

$$\mathrm{SNR} = \frac{\int_0^\infty S_1(\mathrm{w})\mathrm{d}w}{S_2(w=\Omega)} = \frac{\pi(R_1\beta)^2}{4R_0}\left[1 - \frac{(R_1\beta)^2}{2\left({R_0}^2 + 4\Omega^2\right)}\right]^{-1} \tag{16}$$

Fig. 4 reveals the effect of noise intensity on MFPT for different parameters. The observation shows that MFPT decreases monotonously with the increase of noise intensity under different parameters. In addition, the larger the parameter value, the faster the decline. Therefore, a high barrier height, a wide potential spacing or a large damping factor will increase the difficulty of particles passing through the potential well and reduce the escape rate [41,42]. The relationship between SNR and noise intensity D is shown in Fig. 5. Similar to CBSR, the SNR of UCUBSR first increases to the maximum and then decreases with the increase of noise intensity. Fig. 6 gives the three-dimensional graph of SNR, system parameter p and D. With increasing noise intensity D, each p exhibits a maximum SNR under different noise intensities, which is the identifying feature of SR phenomenon. From Fig. 6(b), with the increase of p, the peak value of the SNR decreases and the peak's position shifts slightly to the larger value of D, indicating that the higher the barrier height, the greater the noise intensity required to reach the maximum SNR and achieve optimal coordination. Fig. 7 reveals the three-dimensional graph of SNR, system parameter $u \in [0.2,\ 5]$ and D. SR phenomena in the system occurs as the SNR curve is at the peak, and the maximum SNR gradually increases with the increase of u. Fig. 8 shows the three-dimensional diagram of SNR, damping factor $k \in [0.01,\ 1]$ and D. As parameter k increases, the optimal SNR decreases and the value of D required to reach the optimal SNR increases, which implies that increasing noise intensity D and the damping factor k can limit the appearance of the optimal SNR.

3. The characteristic analysis of SR based on SNR and amplitude gain

At present, most of the papers on CBSR saturation take the SNR of output signal as the evaluation of the system's unsaturation ability. The SNR of a signal is expressed as follows.

$$SNR = 10\log_{10}\left(\frac{Af_t}{\sum_j Af_j - Af_t}\right) \tag{17}$$

where Af_t is the amplitude of the characteristic frequency f_t in power spectrum of the signal and $\sum_j Af_j$ is the sum of all frequency amplitudes.

3.1. Unsaturation index based on amplitude gain

A new evaluation index of unsaturation, amplitude gain S, is proposed in this paper. The expression of S is as follows

$$S = 10\log_{10}\frac{Af_o}{Af_i} \tag{18}$$

where Af_i, Af_o are respectively the amplitude of input signal and output signal at the characteristic frequency. The greater the S, the better the unsaturation performance.

To prove that the amplitude gain can be used as the evaluation index of the unsaturation ability of the SR system separately and effectively, Fig. 9 presents the relationships between the output

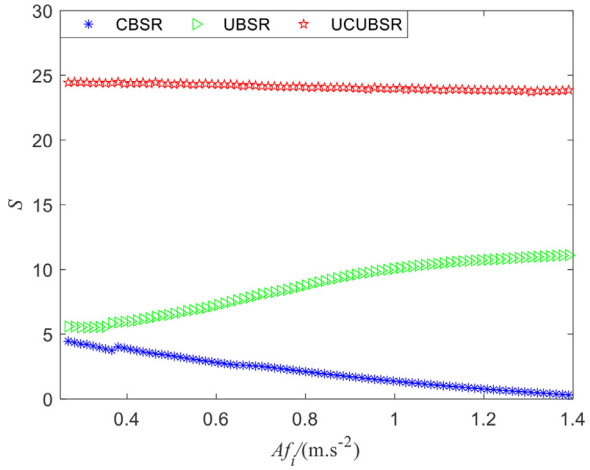

Fig. 11. Curves of the amplitude gain S and Af_i of input signal in different systems.

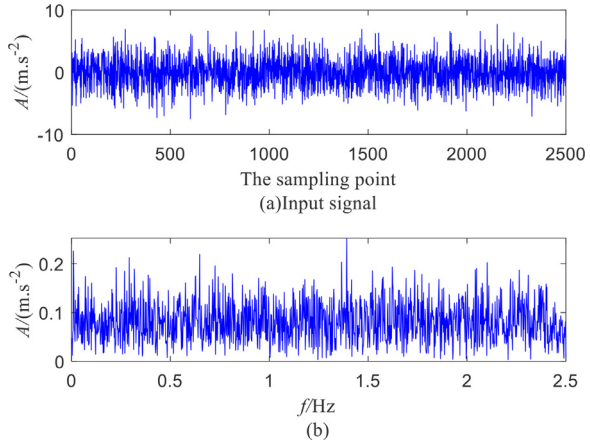

Fig. 12. (a) Time domain waveform and (b) spectra diagram of the input signal.

SNR, amplitude gain S and the noise intensity D for different system parameter l. Firstly, it is well known that the non-monotonic relationship of the SNR and noise intensity D is considered as the recognition characteristic of the existence of SR phenomenon as shown in Fig. 9(a). With the increase of l, the maximum SNR increases and the position of the maximum shifts towards the larger value of D. This implies that enlarge noise intensity D and system parameter l can promote the appearance of the maximum SNR. Then, SR phenomenon in terms of amplitude gain is analyzed in Fig. 9(b). There is always an obvious peak in the amplitude gain curve for $l = 1,\ 1.23$ and 1.26, reflecting the occurrence of SR. The amplitude gain can be considered as an appropriate index to quantify SR. Moreover, according to the definition of the amplitude gain, the feature amplitude enhancement capability of the system first increases and then decreases with the increase of noise intensity, and a bigger l can improve amplitude gain, leading to the promotion of the SR.

3.2. Comparison of unsaturation indexes

This chapter compares the proposed index with SNR in the evaluation of unsaturation ability of the different SR systems. Among them, there are CBSR system, UCUBSR system and unsaturation bistable stochastic resonance (UBSR) system mentioned in [14]. The amplitude of the sinusoidal signal $S(t)$ is increased from 0.3 to 1.5 with a step length of 0.015, totally 81 inputs, and

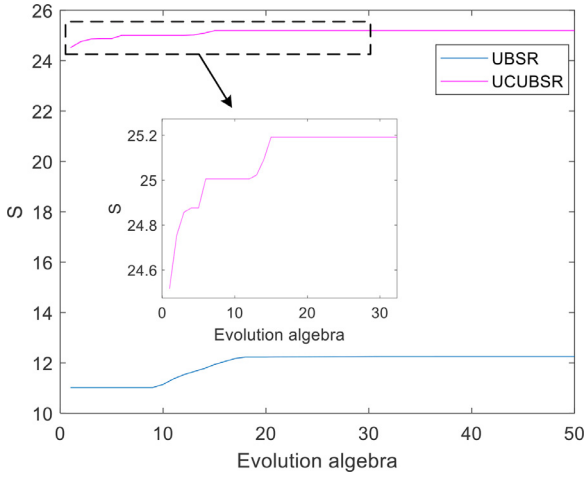

Fig. 13. Iterative process of PSO with S as objective function.

Table 1
Parameter settings in UBSR and UCUBSR.

Input type	Bound	a	b	p	u	l
Analog	Upper	5	5	5	5	$\sqrt{2}$
signal	Lower	0	0	0	0	1
Fault	Upper	5	5	1	5	$\sqrt{2}$
signal	Lower	0	0	0	2	1

the Gaussian white noise $\eta(t)$ with the noise intensity $D = 0.5$ is added. We take the characteristic frequency $f_t = 0.01$ Hz, sampling frequency $f_s = 5$ Hz, sampling length $N = 4096$. The barrier height and the potential spacing of these three systems are the same, which are $\Delta U = 0.25$ and $\Delta L = 2$, respectively. In addition, $l = 1.1,\ k = 0.04$ in UCUBSR system are set. Each input signal is processed by three models to obtain the corresponding output signal. The SNR of the input signal (SNR_{in}) and the SNR of the output signal (SNR_{out}) are calculated by Eq. (17), and the relationship between SNR_{in} and SNR_{out} in each model is shown in Fig. 10.

For the dotted rectangle in Fig. 10, the SNR_{out} of UCUBSR is the largest, followed by UBSR and CBSR in the same input signal. The unsaturation ability of UCUBSR is stronger than that of UBSR and CBSR. However, for the outside of the dotted rectangle in Fig. 10, the SNR_{out} of UCUBSR and UBSR is extremely close. It is not easy to judge the unsaturation performance of the two systems based on SNR. Specifically, when the $S_1(t) = 1.275\sin(2\pi f_t)$, the input signal and the output signals $x_a(t),\ x_b(t)$ and $x_c(t)$ obtained by CBSR, UBSR and UCUBSR are presented in Fig. 10. The SNR_{out} of CBSR, UBSR and UCUBSR are $-13.5898,\ -9.3065,$ and -9.3098, respectively. The latter two values are approximately the same, indicating that the unsaturation ability of UBSR and UCUBSR is equivalent based on SNR index. But the amplitude of output signal of UCUBSR is about 20 times higher than that of UBSR in the time domain diagrams. It can be seen that the SNR is obviously not convincing as an evaluation index of unsaturation ability.

Then, the amplitude gain S of the above 81 groups of input signals processed by three systems is shown in Fig. 11. The S curve of the UCUBSR system is always higher than that of UBSR and CBSR, and there is no crossing between the curves like Fig. 10, which means the unsaturation ability of UCUBSR are the best, followed by UBSR, CBSR is the worst, and also proves the superiority of index S. The amplitude gain S as an evaluation indicator, it not only has a certain compensation effect on the SNR indicator, but also has a good degree of discrimination.

Table 2
Particle swarm optimization results of the analog signal (damping factor $k = 0.04$).

	S_{max}	SNR_{max}	system parameters	Af_o
UBSR	12.2539	/	$a = 0.100, b = 4.9385$	3.799
UCUBSR	25.1923	/	$p = 2.1514, u = 3.6117,$ $l = 1.0803$	74.69
UCUBSR	/	−8.9513	$p = 1.2420, u = 2.3768,$ $l = 1.1162$	71.36

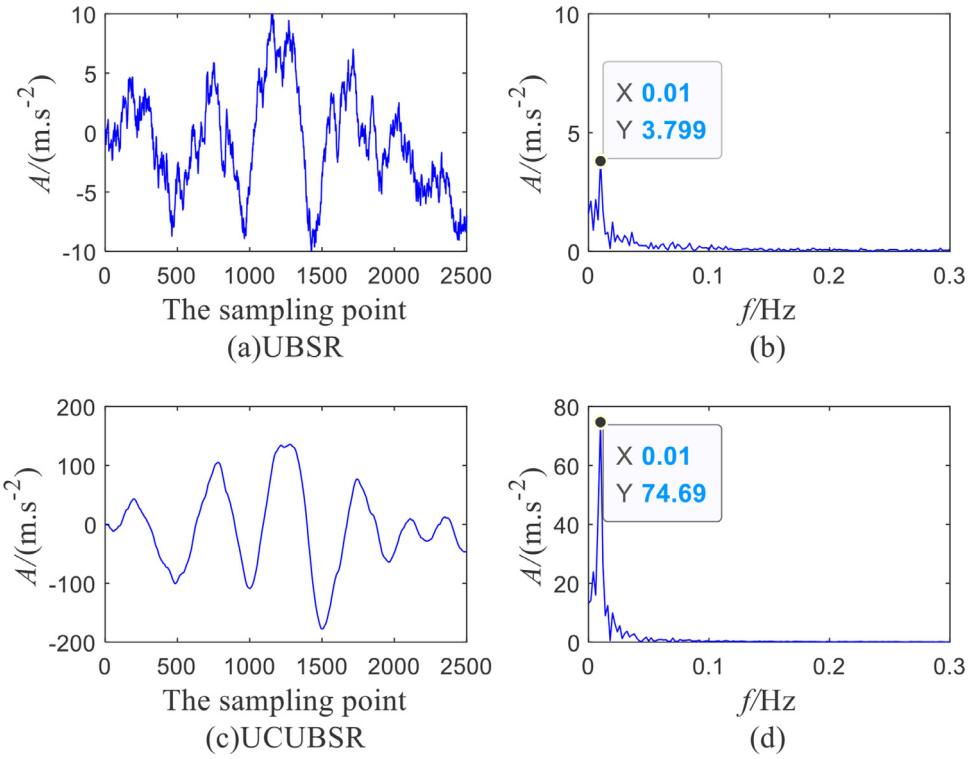

Fig. 14. Comparison of the output signal obtained by UBSR (a) and (b) and UCUBSR (c) and (d).

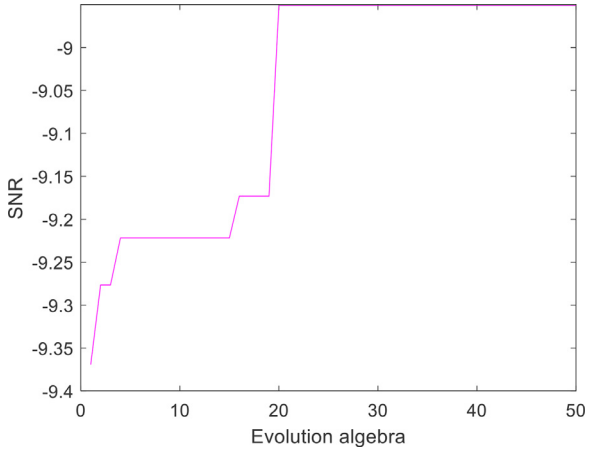

Fig. 15. Iterative process of PSO with SNR as objective function.

4. Simulation analysis and experimental verification

The simulation signal and actual signal are used to verify the reliability of UCUBSR's unsaturation capability and amplitude gain index. For one thing, particle swarm optimization (PSO) is used to adjust system parameters, and the optimal output results of UBSR and UCUBSR are obtained to compare their unsaturation performance. For another thing, the significance of the proposed index S is proved by the optimal output results of analog signal and fault signal in UCUBSR system.

4.1. Parameter optimization by PSO

SR is extremely sensitive to system parameters. Matching system parameters is a vital way to trigger SR. PSO is a random search algorithm and adopted to search the best matching parameter pair of the UBSR system and UCUBSR system. To ensure the convergence of the algorithm, the parameter settings are listed in Table 1. Among them, the parameters of UBSR system are a and b, and p, u and l are UCUBSR system parameters. Each model is optimized 10 times to get 10 best output results, and the maximum value of them is selected as the optimal output value of the model in the algorithm.

4.2. simulation analysis

The signal generated by sine signal $S(t) = 0.2\sin(0.02\pi t)$ and Gaussian white noise with noise intensity $D = 5$ is used as the input signal of SR system. The basic settings are given as follows: sampling frequency $f_s = 5$ Hz and sampling point $N = 2500$. The time-frequency diagram of input signal is shown in Fig. 12. In the spectrum of Fig. 12(b), the amplitude at $f_t = 0.01$ is shielded by vast powerful noise and the frequency at the maximum amplitude

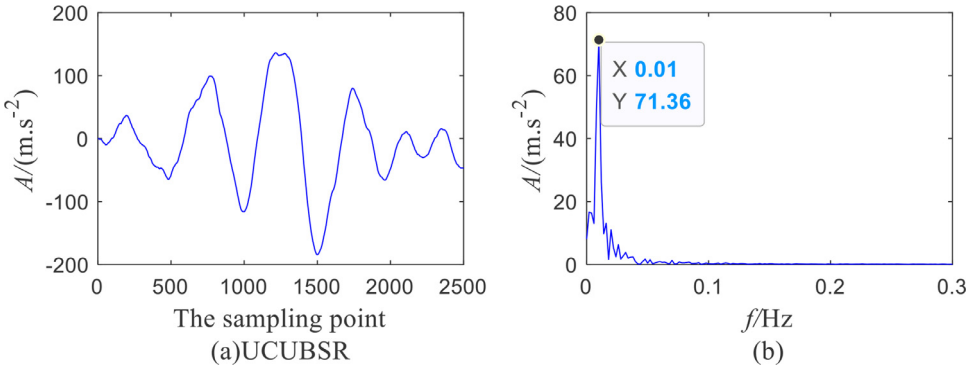

Fig. 16. (a) Time domain waveform and (b) spectra of the output signal.

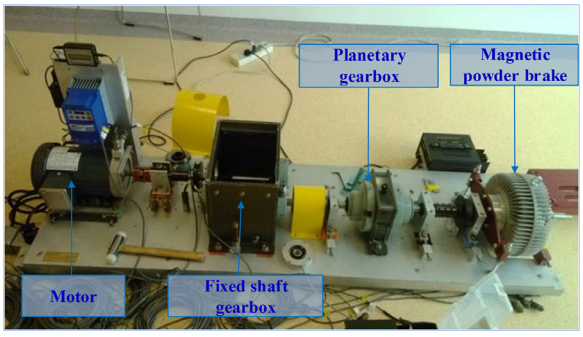

Fig. 17. Experimental platform.

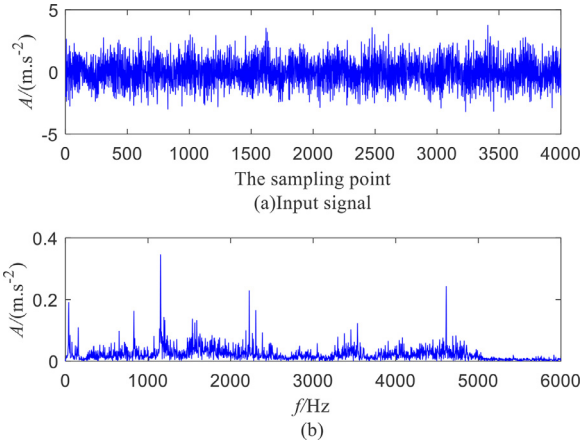

Fig. 18. (a) Time domain waveform and (b) spectra of the bearing outer ring fault signal.

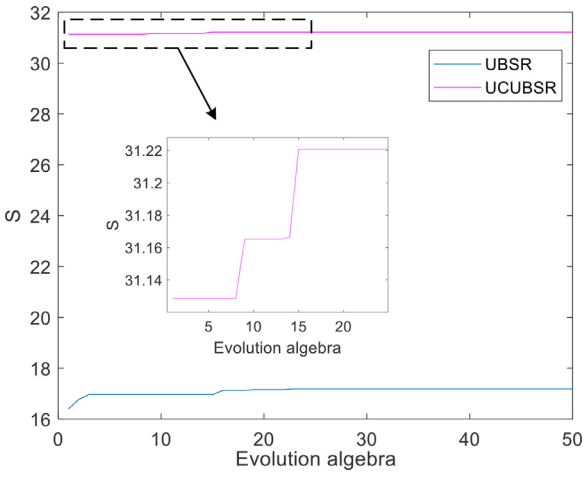

Fig. 19. Iterative process of PSO with S as objective function.

is 1.362 Hz. It is quite difficult to extract the characteristic of the input signal.

To compare the unsaturation capability, PSO is used to optimize the parameters of UBSR and UCUBSR respectively with the amplitude gain S as the objective function. The optimization process of two systems is shown in Fig. 13. The algorithm converges to obtain the optimal amplitude gain (S_{max}). $S_{max} = 12.2539$ and the optimal parameters are $a = 0.100$ and $b = 4.9385$ in UBSR system. $S_{max} = 25.1923$ and the optimal parameters are $p = 2.1514, u = 3.6117$ and $l = 1.0803$ in UCUBSR system. Based on the S_{max}, the output signals are presented in Fig. 14. There exists a peak at the characteristic frequency in the spectrum diagrams in Fig. 14(b) and (d), illustrating that both systems can extract the feature of the weak signal. In addition, the S_{max} of UCUBSR system is 12.9384 higher than that of UBSR system, and the amplitude of output signal at characteristic frequency Af_o is 3.799 in UBSR system and 74.69 in UCUBSR system respectively. These indicate the proposed system improves the ability of weak signal feature enhancement and is better than the UBSR system in the unsaturation ability. The optimization results are compared in Table 2.

Then, to illustrate the significance of the proposed evaluation index, the output SNR is selected as the objective function of PSO algorithm to optimize the above analog signal in UCUBSR system. The search process is given in Fig. 15, and the optimal result SNR_{max} is -8.95 and the corresponding parameters are $p = 1.2420$, $u = 2.3768$, $l = 1.1162$. After optimization, the time-frequency diagram of the output signal is obtained in Fig. 16. Obviously, the characteristic frequency $f_t = 0.01$ Hz of the power spectrum is detected with maximum amplitude $Af_o = 71.36$. Furthermore, the Af_o in Fig. 14(d) is 3.3 bigger than that in Fig. 16(b). This shows that the amplitude gain further guides the parameter adjustment of SR, making the proposed system amplify in enhancement of feature extraction effect. The system processing results are summarized in Table 2.

4.3. Experimental verification

The bearing fault signal was collected on the experimental platform in Fig. 17, in which the outer ring of medium speed shaft bearing was in fault. The model of the bearing applied in the experiment was EK-16k. The test point was the middle speed end near the motor end. The speed ratio and load ratio are both 80%. The experimental setup is as below: the motor speed is 2400 r/min, the sampling frequency is set to 1.2 K Hz and the

Table 3
Particle swarm optimization results of the bearing outer ring fault signal (damping factor $k = 0.04$).

	S_{max}	SNR_{max}	system parameters	Af_o
UBSR	17.1958	/	$a = 0.100, b = 2.0907$	9.984
UCUBSR	31.2207	/	$p = 0.1235, u = 3.2678,$ $l = 1.4142$	251.6
UCUBSR	/	−11.2257	$p = 0.3933, u = 4.2480,$ $l = 1.0767$	227

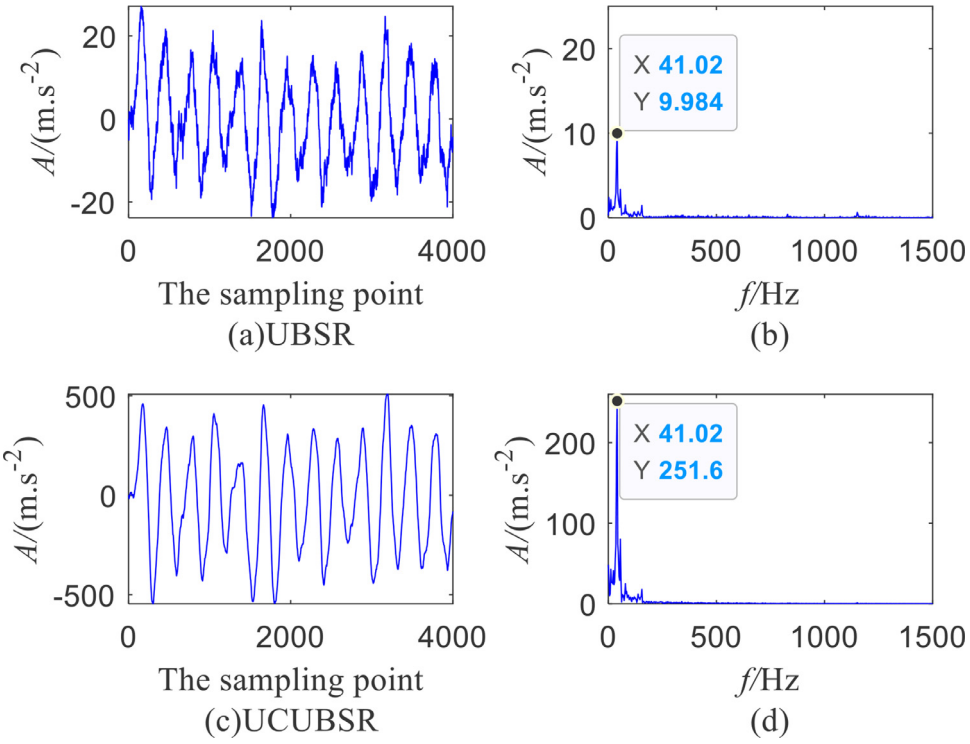

Fig. 20. Comparison of the fault output signal obtained by UBSR (a) and (b) and UCUBSR (c) and (d).

sampling lasts 6 s. The first 4096 data of working condition 29 are selected as the fault signal to be tested. To satisfy the small parameter limit of SR, the secondary sampling frequency is fixed as 0.9 Hz [38]. The time-frequency diagram of the bearing outer ring fault signal is given in Fig. 18. In the spectrum diagram Fig. 18(b), the frequency with the peak is 1151 Hz, the frequency range gets wide, and the energy is mainly concentrated in the high frequency interference region. Apparently, the fault frequency $f_{BFPO} = 41.435$ Hz cannot be distinguished due to the presence of strong background noise.

Firstly, taking the amplitude gain S as the objective function of PSO algorithm, the fault signal is processed by the UBSR system and UCUBSR system. Fig. 19 shows the process of searching the optimal result, and the optimization results of the bearing outer ring fault signal are compared in Table 3. The optimal result $S_{max} = 17.1958$ and the corresponding parameters are $a = 0.100$ and $b = 2.0907$ in UBSR system. $S_{max} = 31.2207$ and the optimal parameters are $p = 0.1235$, $u = 3.2678$ and $l = 1.4142$ in UCUBSR system. The output time-frequency diagram of the two systems is given in Fig. 20. The output signal has a certain periodicity in Fig. 20(a) and (c). Then, by observing Fig. 20(b) and (d), the energy of high frequency interference signal is transmitted to the bearing outer ring fault signal through SR to highlight the fault characteristics, and a distinct peak appears at the frequency 41.02 approximately closed to the fault frequency, indicating that fault feature is clearly detected. Moreover, the S_{max} of UCUBSR system is 14.0249 higher than that of UBSR system and the Af_o of UCUBSR system is nearly 25.2 times bigger than that of UBSR system. These demonstrate that the proposed method can alleviate the saturation problem more effectively and is better at detecting weak fault features in strong noisy background.

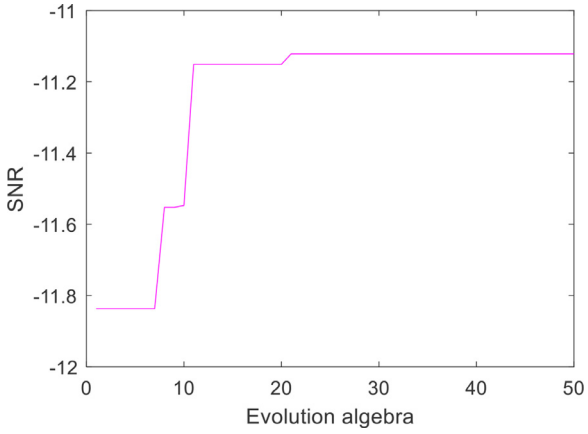

Fig. 21. Iterative process of PSO with SNR as objective function.

Then, to further prove the importance of the proposed index S, the output SNR is taken as the objective function in UCUBSR system. Fig. 21 reveals the search process of maximum output SNR $SNR_{max} = -11.2257$ and the optimal parameters $p = 0.3933$, $u = 4.2480$, $l = 1.0767$. The optimized output signal is presented in

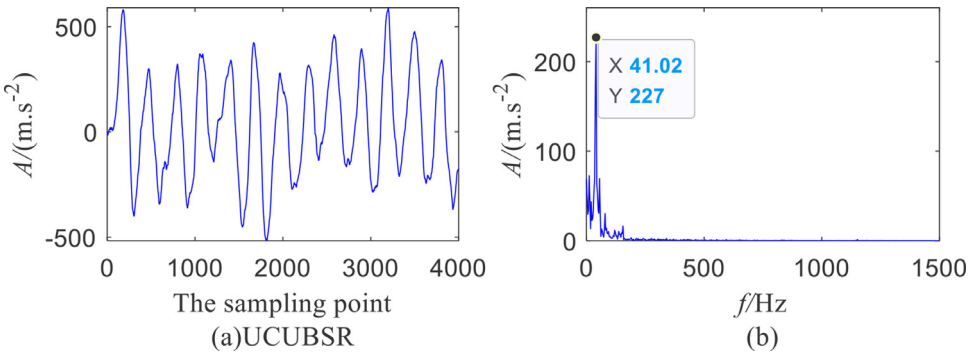

Fig. 22. (a) Time domain waveform and (b) spectra of the fault output signal.

Fig. 22, where the fault frequency 41.02 Hz with a pronounced peak $Af_o = 227$ in the power spectrum is notably highlighted. Compared with Fig. 22(b), the $Af_o = 251.6$ of the bearing outer ring fault signal in Fig. 20(d) is increased by 24.6. Thus, the frequency domain feature can be effectively enhanced when the amplitude gain S is taken as objective function. Briefly, the UCUBSR system with the amplitude gain S as objective function of the optimization algorithm can further improve amplification performance of system fault characteristic signal and facilitate bearing fault identification.

5. Conclusion

In conclusion, an underdamped continuous unsaturation bistable stochastic resonance system is put forward, and the effectiveness and superiority of the proposed system in weak fault feature extraction are studied by theoretical simulation and experimental analysis. The research shows that:

To overcome the saturation problem of CBSR system, a new potential function model is constructed, which can adjust the barrier height ΔU, potential spacing ΔL and steepness l independently. The SNR of the UCUBSR system is derived.

An improved evaluation index amplitude gain S is proposed. The effect of the system parameter l on SR based on SNR and amplitude gain demonstrates that the S is a suitable indicator for quantifying the SR. In addition, the simulation analysis proves that the S can make up for the deficiency of SNR as an evaluation index and has a good degree of discrimination.

In the simulation and bearing fault experiment, the amplitude gain is taken as the objective function of PSO. Compared with UBSR system, the UCUBSR system has larger amplitude gain. This proves that the proposed system has better ability of the unsaturation and weak fault characteristic enhancement.

In UCUBSR system, the higher output amplitude at characteristic frequency indicates the amplitude gain S can further guide the parameter adjustment of SR and enhance the amplitude enhancement ability of SR system, which is conducive to weak fault detection

CRediT author statement

Mengdi Li: Methodology, Software, Formal analysis, Writing-Original draft preparation.

Peiming Shi: Conceptualization, Data curation, Project administration, Writing - Review & Editing

Wenyue Zhang: Investigation, Visualization

Dongying Han: Resources, Writing- Reviewing and Editing

Declaration of Competing Interest

The authors declare that they have no conflict of interest.

Acknowledgments

The studies were funded by the National Natural Science Foundation of China (Grant numbers 61973262 and 51875500), Project of introducing overseas talents in Hebei Province (C20190371) and The central government guides local science and technology development fund projects (216Z4301G, 216Z2102G).

References

[1] Benzi R, Sutera A, Vulpiani A. The mechanism of stochastic resonance. J Phys A 1981;14:453–7.
[2] Mcnamara B, Wiesenfeld K, Roy R. Observation of stochastic resonance in a ring laser. Phys Rev Lett 1988;60:2626–9.
[3] Douglass JK, Wilkens L, Pantazelou E, Moss F. Noise enhancement of information-transfer in crayfish mechanoreceptors by stochastic resonance. Nature 1993;365:337–40.
[4] Zeng F, Fu Q, Morse R. Human hearing enhanced by noise. Brain Res 2000;869:251–5.
[5] Spagnolo B, Barbera ALa. Role of the noise on the transient dynamics of an ecosystem of interacting species. Physica A 2002;315:114–24.
[6] Zhang WY, Shi PM, Li MD, et al. A novel stochastic resonance model based on bistable stochastic pooling network and its application. Chaos Soliton Fract 2021;145:110800.
[7] Lu SL, He QB, Wang J. A review of stochastic resonance in rotating machine fault detection. Mech Syst Sig Process 2019;116:230–60.
[8] Yang C, Yang J, Zhu Z, Shen G, et al. Distinguish coherence resonance and stochastic resonance in bearing fault evaluation. Meas Sci Technol 2020;31:045001.
[9] Rousseau D, Varela JR, Chapeau-Blondeau F. Stochastic resonance for nonlinear sensors with saturation. Phys Rev E 2003;67:021102.
[10] Qiao ZJ, Liu J, Ma X, et al. Double stochastic resonance induced by varying potential-well depth and width. J Franklin I 2021 in press.
[11] Liu J, Hu B, Yang F, et al. Stochastic resonance in a delay -controlled dissipative bistable potential for weak signal enhancement. Commun Nonlinear Sci 2020;85:105245.
[12] Zhao S, Shi PM, Han DY. A novel mechanical fault signal feature extraction method based on unsaturated piecewise tri-stable stochastic resonance. Measurement 2021;168:108374.
[13] Zhao WL, Wang J, Wang LZ. The unsaturated bistable stochastic resonance system. Chaos 2013;23:033117.
[14] Qiao ZJ, Lei YG, Lin J, et al. An adaptive unsaturated bistable stochastic resonance method and its application in mechanical fault diagnosis. Mech Syst Signal Process 2017;84:731–46.
[15] Zhang G, Hu DY, Zhang TQ. Stochastic resonance in unsaturated piecewise nonlinear bistable system under multiplicative and additive noise for bearing fault diagnosis. IEEE Access 2019;7:58435–48.
[16] Li JM, Wang XD, Wu H. Rolling bearing fault detection based on improved piecewise unsaturated bistable stochastic resonance method. IEEE T Instrum Meas 2020:6501309.
[17] Dong HT, Shen XH, He K, et al. Nonlinear filtering effects of intrawell matched stochastic resonance with barrier constrainted duffing system for ship radiated line signature extraction. Chaos Soliton Fract 2020;141:110428.
[18] Lopez C, Zhong W, Lu SL, et al. Stochastic resonance in an underdamped system with FitzHug-Nagumo potential for weak signal detection. J Sound Vib 2017;411:34–46.
[19] Guo F, Cheng XF, Wang SL, et al. Behavior of stochastic resonance for an underdamped bistable system driven by multiplicative and additive signals. Phys Scripta 2021;96:015001.
[20] Zhang WY, Shi PM, Li MD, et al. Signal detection based on second-order underdamped tristable stochastic resonance and Its Application to Weak Fault Diagnosis. IEEE Access 2019;7:173753–65.

[21] Li ZX, Liu XD, Wang XR, et al. A multi-parameter constrained potential underdamped stochastic resonance method and its application for weak fault diagnosis. J Sound Vib 2019;459:114862.
[22] Giuffrida A, Valenti D, Ziino G, et al. A stochastic interspecific competition model to predict the behaviour of Listeria monocytogenes in the fermentation process of a traditional Sicilian salami. Eur Food Res Technol 2009;228:767–75.
[23] Denaro G, Valenti D, Cognata ALa, et al. Spatio-temporal behaviour of the deep chlorophyll maximum in Mediterranean Sea: development of a stochastic model for picophytoplankton dynamics. Ecol Complex 2013;13:21–34.
[24] Pizzolato N, Fiasconaro A, Persano Adorno D, et al. Resonant activation in polymer translocation: new insights into the escape dynamics of molecules driven by an oscillating field. Phys Biol 2010;7:034001.
[25] Ando B, Baglio S, Bulsara AR, et al. A nonlinear energy harvester operated in the stochastic resonance regime for signal detection/measurement applications. IEEE T Instrum Meas 2020;69:5930–40.
[26] Han DY, Shi PM. Study on the mean first-passage time and stochastic resonance of a multi-stable system with colored correlated noises. Chinese J Phys 2021;69:98–107.
[27] Wang KK, Ju L, Wang YJ, et al. Impact of colored cross-correlated non-Gaussian and Gaussian noises on stochastic resonance and stochastic stability for a metapopulation system driven by a multiplicative signal. Chaos Soliton Fract 2018;108:166–81.
[28] Kim H, Tai WC, Parker J, et al. Self-tuning stochastic resonance energy harvesting for rotating systems under modulated noise and its application to smart tires. Mech Syst Sig Process 2019;122:769–85.
[29] He MJ, Xu W, Sun ZK, et al. Characterization of stochastic resonance in a bistable system with Poisson white noise using statistical complexity measures. Commun Nonlinear Sci Numer Simulat 2015;28:39–49.
[30] He MJ, Xu W, Sun ZK, et al. Characterizing stochastic resonance in coupled bistable system with Poisson white noises via statistical complexity measures. Nonlinear Dyn 2017;88:1163–71.
[31] Huang DW, Yang JH, Zhou DJ, et al. Novel adaptive search method for bearing fault frequency using stochastic resonance quantified by amplitude-domain index. IEEE T Instrum Meas 2020;69:109–21.
[32] Huang DW, Yang JH, Zhou DJ, et al. Recovering an unknown signal completely submerged in strong noise by a new stochastic resonance method. Commun Nonlinear Sci 2019;66:156–66.
[33] He MJ, Xu W, Sun ZK. Dynamical complexity and stochastic resonance in a bistable system with time delay. Nonlinear Dyn 2015;79:1787–95.
[34] Xu PF, Jin YF. Stochastic resonance in an asymmetric tristable system driven by correlated noises. Appl Math Model 2020;77:408–25.
[35] Wang S, Wang FZ, Wang S, et al. Detection of multi-frequency weak signals with adaptive stochastic resonance system. Chin J Phys 2018;56:994–1000.
[36] Hu BB, Li B. Blade crack detection of centrifugal fan using adaptive stochastic resonance. Shock Vib 2015:954932.
[37] Xiao L, Bajric R, Zhao JS, et al. An adaptive vibrational resonance method based on cascaded varying stable-state nonlinear systems and its application in rotating machine fault detection. Nonlinear Dyn 2021;103:715–39.
[38] Li MD, Shi PM, Zhang WY, et al. Study on the optimal stochastic resonance of different bistable potential models based on output saturation characteristic and application. Chaos Soliton Fract 2020;139:110098.
[39] Zhang G, Zhang YJ, Zhang TQ, et al. Stochastic resonance in second-order underdamped system with exponential bistable potential for bearing fault diagnosis. IEEE Access 2018;6:42431–44.
[40] Gammaitoni L, Hanggi P, Jung P. Stochastic resonance. Rev Mod Phys 1998;86:223–87.
[41] Fiasconaro A, Valenti D, Spagnolo B. Role of the initial conditions on the enhancement of the escape time in static and fluctuating potentials. Physica A 2003;325:136–43.
[42] Spagnolo B, Dubkov AA, Agudov NV. Enhancement of stability in randomly switching potential with metastable state. Eur Phys J B 2004;40:273–81.